

Stabilizing Surface Passivation Enables Stable Operation of Colloidal Quantum Dot Photovoltaic Devices at Maximum Power Point in an Air Ambient

Jongmin Choi, Min-Jae Choi, Junghwan Kim, Filip Dinic, Petar Todorovic, Bin Sun, Mingyang Wei, Se-Woong Baek, Sjoerd Hoogland, F. Pelayo García de Arquer, Oleksandr Voznyy, and Edward H. Sargent*

Colloidal quantum dots (CQDs) are promising materials for photovoltaic (PV) applications owing to their size-tunable bandgap and solution processing. However, reports on CQD PV stability have been limited so far to storage in the dark; or operation illuminated, but under an inert atmosphere. CQD PV devices that are stable under continuous operation in air have yet to be demonstrated—a limitation that is shown here to arise due to rapid oxidation of both CQDs and surface passivation. Here, a stable CQD PV device under continuous operation in air is demonstrated by introducing additional potassium iodide (KI) on the CQD surface that acts as a shielding layer and thus stands in the way of oxidation of the CQD surface. The devices (unencapsulated) retain >80% of their initial efficiency following 300 h of continuous operation in air, whereas CQD PV devices without KI lose the amount of performance within just 21 h. KI shielding also provides improved surface passivation and, as a result, a higher power conversion efficiency (PCE) of 12.6% compared with 11.4% for control devices.

Colloidal quantum dots (CQDs) are attractive semiconductor materials owing to their size tunable bandgap, solution processing, and ambient stability.^[1–3] These benefits have enabled the application of CQDs in thin-film optoelectronic devices such as light emitting diodes,^[4,5] transistors,^[6,7] photodetectors,^[8,9]

and photovoltaics (PV).^[10–13] Progress in CQD devices has been achieved through advanced surface chemistry, energy band engineering combined with device architecture optimization,^[14–17] and these combined have produced certified power conversion efficiencies (PCEs) of 12%.^[18]

A remaining challenge for the field is to improve the stability under device operation conditions. Bare CQDs are unstable in air: they are readily oxidized due to the high surface-to-volume ratio.^[19–21] Stability of CQD solids have been improved via halide anion passivation, which protects the surface of CQDs from the effects of oxygen.^[19–21] Among halide anions, iodide is the most effective protectant due to its large atomic radius.^[19]


Recent advances in CQD PV have relied on lead iodide (PbI₂) passivated CQD solids fabricated using solution-based ligand exchanges, with devices retaining 90% of their initial performance following air storage for 1000 h.^[12] With the additional help of hydro/oxo-phobic hole transporting materials, the air stability retained over 90% of initial performance following 1 year of ambient air storage.^[22] Cao et al. reported that CQD PV devices retain 80% of their initial efficiency following 1000 h of continuous light illumination under N₂ atmosphere.^[23]

Despite impressive progress in CQD device stability, most of these achievements relied on the measurements under long-term air storage or light illumination without electric load, which are still far from device operation conditions. To realize the full potential of CQDs in a PV device, they should retain their performance under maximum power point (MPP) conditions, which still remains an open challenge. Recently, Zhang et al. reported CQD PV device that preserves around 88% of its initial efficiency after 46 h of MPP aging.^[24] However, the result was performed under a nitrogen atmosphere, while the MPP stability under air ambient is presumably significantly worse. To date, though, device operational stability of CQD PV device in air has not yet to be fully addressed.

Herein we link stable device performance under continuous operation in air to our deployment of a potassium iodide (KI) shielding layer. We find that KI protects both the CQDs and

Prof. J. Choi,^[†] Dr. M.-J. Choi, Dr. J. Kim,^[††] P. Todorovic, Dr. B. Sun, M. Wei, Dr. S.-W. Baek, Dr. S. Hoogland, Dr. F. P. García de Arquer, Prof. E. H. Sargent
Department of Electrical and Computer Engineering
University of Toronto
10 King's College Road, Toronto, Ontario M5S 3G4, Canada
E-mail: ted.sargent@utoronto.ca

F. Dinic, Prof. O. Voznyy
Department of Physical and Environmental Sciences
University of Toronto
1065, Military Trail, Toronto, Ontario M1C 1A4, Canada

 The ORCID identification number(s) for the author(s) of this article can be found under <https://doi.org/10.1002/adma.201906497>.

^[†]Present address: Department of Energy Science and Engineering, Daegu Gyeongbuk Institute of Science and Technology (DGIST), Daegu 72988, Republic of Korea

^[††]Present address: Photo-electronic Hybrids Research Center, Korea Institute of Science and Technology (KIST), Seoul 02792, Republic of Korea

DOI: 10.1002/adma.201906497

the surface passivation of CQDs against oxidation and thus allows them to retain their original surface chemistry. Specifically, devices retain $\approx 80\%$ of their initial PCE following 300 h of continuous operation in air; whereas CQD PV devices without KI retain 80% of initial PCE only for 21 h at MPP. In addition, KI shielding enables higher loading of iodide, resulting in increased carrier transport and higher PCE (12.6%) than in control devices (11.4%).

We first explored the MPP stability of the state-of-the-art CQD PV devices that are using PbI_2 -passivated CQD films,^[12,18] investigating the evolution of performance in time in an air ambient. The device configuration is ITO/ZnO/PbS– PbI_2 /PbS–1,2-ethanedithiol (EDT)/Au, where ZnO layer is the electron transport layer, PbS– PbI_2 layer is the light harvesting layer, and PbS–EDT layer acts as a hole transport layer. The device

retained 75% of its initial performance following 50 h MPP operation in air (Figure 1a,b). We note in light of previous studies of dark air storage^[12] and illuminated N_2 operation,^[23] devices are less stable under continuous operation at MPP condition in air compared to the previously studied scenarios.

We carried out X-ray photoelectron spectroscopy (XPS) measurements of CQD films to reveal the origin of this degradation, and found that oxygen is increased and iodide is reduced (Figure 1c,d, and Table S1, Supporting Information). XPS O 1s spectra show the formation of PbO, PbSO_3 , and PbSO_4 in CQD films under continuous external photostress in air. A slight increase in V_{oc} after 50 h MPP operation can be attributed to oxides that induce p-type character in CQDs.^[25–27] Based on these findings, combined with the thermochemistry of Pb, whose Gibbs free energy of Pb–O interaction ($\Delta G_{\text{PbO}}^{\text{O}} = -189.24 \text{ kJ mol}^{-1}$) is

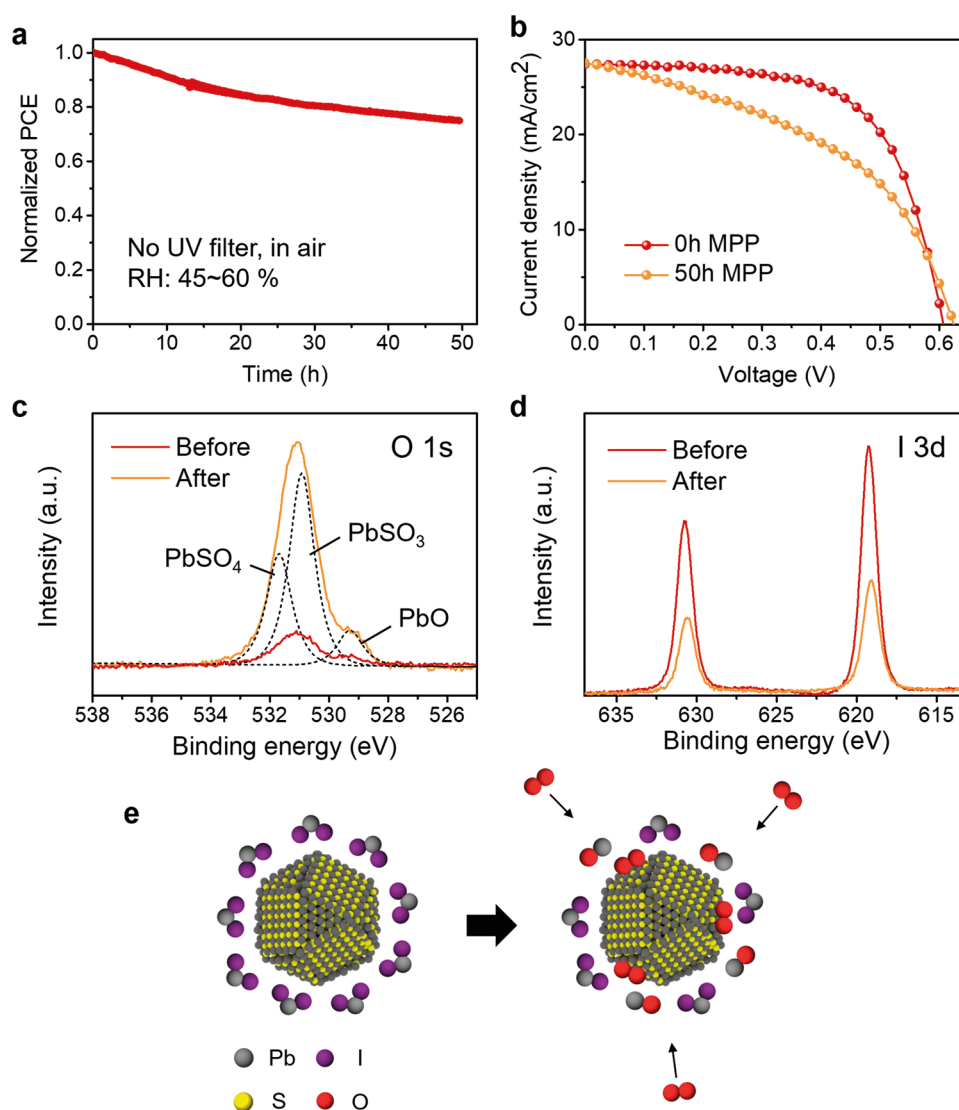


Figure 1. Maximum power point (MPP) stability of PbI_2 -passivated PbS CQD PV devices under an air ambient. a) MPP tracking for 50 h of unencapsulated devices under continuous 1 sun illumination, $50 \pm 10\%$ relative humidity, at room temperature. b) Current density–voltage (J – V) characteristics of devices in (a) before versus after MPP aging. c) XPS O 1s spectra and d) XPS I 3d spectra of PbI_2 -passivated CQD solids before and after AM1.5 illumination for 30 h in air. Dashed lines indicate the different chemical bonding states of oxygen (529.3 eV for PbO, 530.9 eV for PbSO_3 , and 531.7 eV for PbSO_4).^[25] e) Schematic illustration of the degradation process of PbI_2 -passivated PbS CQD solids by oxidation.

lower than that of Pb–I ($\Delta G_{\text{PbI}_2}^{\text{O}} = -173.59 \text{ kJ mol}^{-1}$), we conclude the degradation process of PbI_2 -passivated CQD solids as shown in Figure 1e: PbI_2 surface passivation degrades to PbO , and PbS CQDs are oxidized to PbSO_3 and PbSO_4 .

We explored agents that could protect the surface from oxidation with the goal of improving MPP stability of devices. We used potassium (K) reasoning that it has a low electron affinity, strong interaction with iodide, and large size, allowing for effective protection of the surface. In addition, it has more stable formation with iodide ($\Delta G_{\text{KI}}^{\text{O}} = -322.29 \text{ kJ mol}^{-1}$) than oxygen ($\Delta G_{\text{K}_2\text{O}}^{\text{O}} = -240.58 \text{ kJ mol}^{-1}$).

We carried out density functional theory (DFT) simulations to test a number of competing hypotheses relative to control studies. Molecular physisorption is the required first step for the conversion of O_2 into oxide. We thus performed a molecular dynamics run of a configuration in which O_2 is physisorbed on a PbS CQD passivated by either PbI_2 (control) or PbI_2 with an addition of KI. Right panels in Figure 2a,b show a cross-sectional image of CQDs in stable final configuration. Initially, for both passivation we observe O_2 embedding into the top surface monolayer, resulting in the coordination of O_2 by 2–3 cations. However, the O_2 molecule remains labile and can diffuse across the surface. In the case of PbI_2 passivation, we observe that O_2 locks in place once it touches the S atom (Figure 2a). An additional simulation comparing O_2 physisorption on an open Pb site versus S site revealed a 0.6 eV stronger physisorption on the S site, providing an easy path for further O_2 splitting and the formation of SO_x , consistent with the observation of PbSO_3

and PbSO_4 in Figure 1c. For the passivation of PbI_2 with KI, KI forms an additional buffer layer protecting the subsurface S sites and thus preventing oxidation of CQD (Figure 2b).

We therefore sought to introduce experimentally a KI shielding layer on the PbI_2 surface passivation of CQDs. We explored various molar ratios of KI added to PbI_2 solution in dimethylformamide (DMF) as the exchange solution. We then carried out solution-phase ligand exchange on oleic acid-capped PbS CQDs (dissolved in octane), resulting in the formation of CQD inks through phase transfer to DMF.

The K 2p spectra indicate K on KI-shielded PbS CQD solids (KPbS), but none on control CQD solids passivated with only PbI_2 (Figure 2c). The amount of iodide on the CQD surface increases in proportion with KI concentration, while oxygen is decreased when KI concentration is increased (Figure 2d). We posit that KI may allow denser iodide passivation, resulting in decreased oxygen on the surface, potentially contributing to improved device performance and stability. Time-resolved photoluminescence studies reveal that KI-CQD inks exhibit 1.2× longer carrier lifetime than control CQD inks, in agreement with improved CQD passivation (Figure S1, Supporting Information).

We also studied the linewidth associated with the excitonic feature in PbS CQD films prepared using different ratios of KI (Figure 2e). KPbS CQD films exhibited a narrower exciton peak and a smaller full-width at half-maximum (FWHM) compared to control PbS CQD films. We offer that band tailing associated with partial CQD aggregation may be reduced in KPbS. However, when the concentration of KI in KPbS exceeds

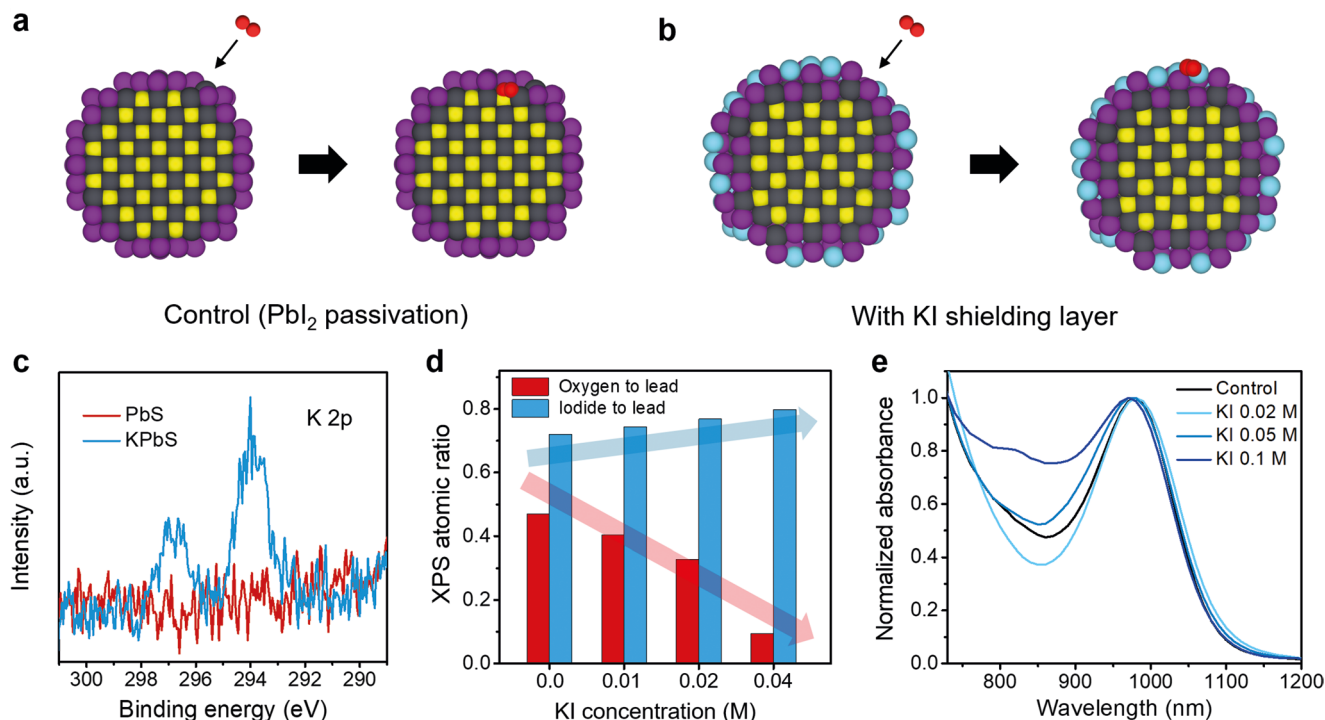


Figure 2. KI-shielded PbS CQD solids. a,b) Reaction of oxygen at the surface of CQDs passivated by PbI_2 (a) and PbI_2 with KI (b). The right images for (a) and (b) are the stable final configurations. While oxygen binds with sulfur in the PbI_2 passivation (a), oxygen cannot contact with sulfur in the KI-shielded passivation (b). The black dots represent Pb atoms, the yellow dots represent S atoms, the wine dots represent I atoms, the red dots represent O atoms, and the light-blue dots represent K atoms. c) XPS K 2p spectra of control PbI_2 -passivated CQD solid (PbS) and KI-shielded CQD solid (KPbS). d) Atomic ratio of oxygen and iodide (referenced to lead) and e) normalized optical absorbance of the KPbS CQD solids with different amounts of KI.

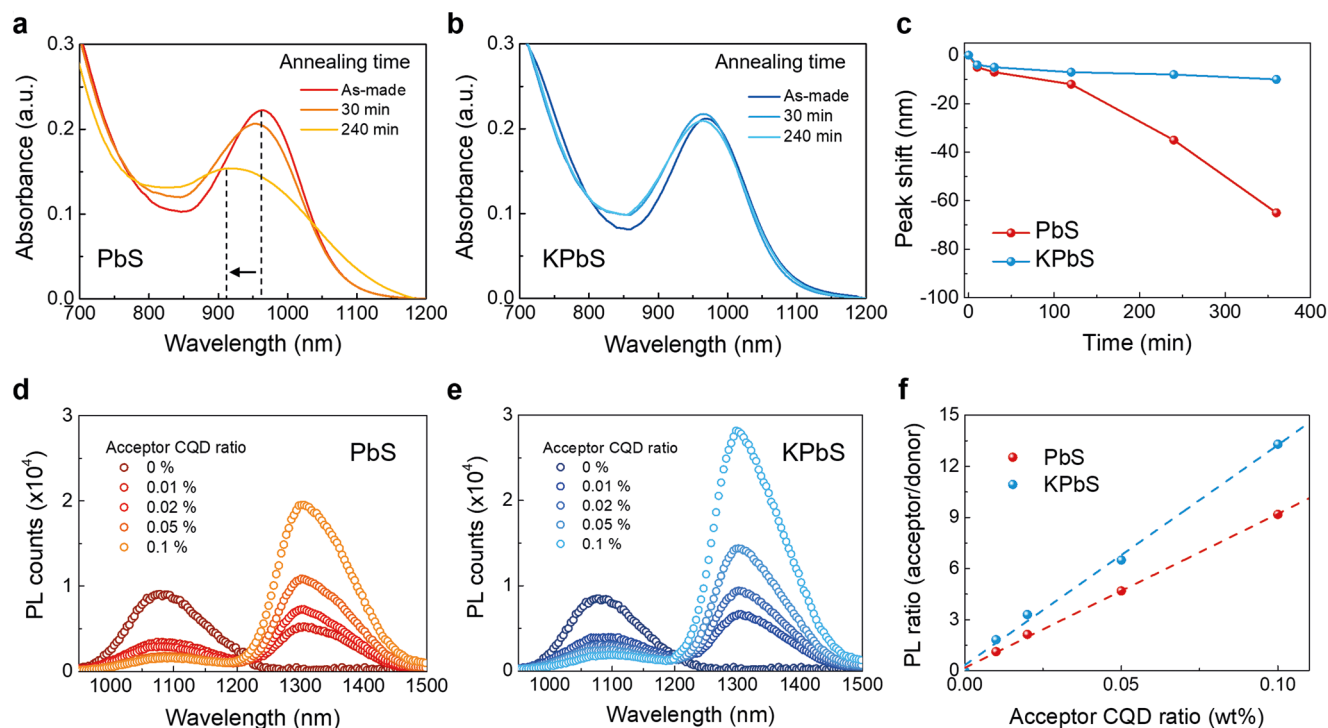


Figure 3. Characterization of KPbS solids. a,b) Absorbance spectra of PbS CQD solids (a) and KPbS CQD solids (b) depending on annealing time at 85 °C. c) Shift of first excitonic peak position of CQD films with annealing. d,e) Photoluminescence (PL) of PbS CQD solids (d) and KPbS CQD solids (e) with various mixture ratios of donor CQD and acceptor CQD. f) Extracted PL ratio (acceptor to donor) of PbS CQD films and KPbS CQD films.

certain amounts, it induces broader exciton peak with a higher FWHM. This is attributed to a thick KI shell formation on PbS CQD surface, suggesting that optimized KI amount (0.02 M) is required in this system. Henceforth, we call PbS CQDs prepared with the optimized KI amounts (0.02 M) as a KPbS CQDs.

To investigate the stability of KPbS CQD films against oxidation, we monitored a change of the absorbance spectra of CQD films following annealing (85 °C) in air. The control PbS CQD films show a dramatic blueshift of excitonic peak after annealing in air, a finding we assign to oxidation that produces oxides and decreases the effective size of PbS CQDs (Figure 3a).^[27,28] The KPbS CQD films exhibit no appreciable shift of excitonic peak position (Figure 3b,c).

We then carried out photoluminescence-based diffusion length measurements on CQD films to compare transport properties between PbS versus KPbS CQD films.^[29] CQD films were prepared using a mixture of two differently sized families of CQDs: bandgap 1.3 eV (donor) and 1.0 eV (acceptor). The PL intensity of the acceptors is increased due to carrier transfer from donors, and the PL intensity of the donors is correspondingly quenched (Figure 3d, e). The PL intensity ratio of acceptor to donor CQDs is thus linked with the diffusion of charges in the donor matrix to the acceptors.^[29] We plotted PL intensity ratio of acceptor to donor as a function of the donor:acceptor ratio (Figure 3f). The KPbS CQD films exhibit a higher PL intensity ratio than do control PbS CQD films, indicating increased mobility of charge carriers.

We also characterized the charge carrier mobility of CQD solids with different KI concentrations using field-effect transistor (FET) measurements. KPbS CQD solids (0.02 M of KI

have a higher electron mobility than do PbS CQD solids; further increases in KI concentration ultimately produce a reduced electron mobility (Figure S2, Supporting Information), in agreement with above FWHM studies.

We then fabricated CQD PV devices employing KPbS. The device architecture of Figure 4a was employed: ITO/ZnO/KPbS/PbS-EDT/Au. The best-performing device with KPbS exhibited a PCE of 12.6% (with a V_{OC} of 0.64 V, a J_{SC} of 28.8 mA cm⁻², and a fill factor (FF) of 69%) compared to 11.4% (with a V_{OC} of 0.64 V, a J_{SC} of 28.0 mA cm⁻², and a FF of 64%) for control PbS devices (Figure 4b). Device histogram shows that KPbS devices exhibit reproducibly higher efficiencies than do PbS devices (Figure S3, Supporting Information). To explore dynamics of charge carriers of the devices, we carried out transient photovoltage (TPV) measurements. KPbS devices exhibit a longer TPV decay time compared to control PbS devices (Figure S4, Supporting Information). This suggests that KPbS reduces charge recombination rates, leading to improved J_{SC} and FF. External quantum efficiency (EQE) spectra (Figure 4c) confirm the enhanced J_{SC} value of KPbS device (28.4 mA cm⁻²) and, in particular, an EQE value exceeding 70% at the excitonic peak, compared with PbS controls exhibiting J_{SC} of 27.5 mA cm⁻².

The operating stability at MPP in air is shown in Figure 5. The PbS CQD PV devices retain around 91% of their initial PCE after 800 h of storage in air without encapsulation (Figure 5a), as we seen in prior reports.^[12] The KPbS CQD PV devices exhibit no performance loss under the same storage conditions. MPP tracking studies widen the gap between PbS versus KPbS CQDs. We observed no performance loss of KPbS CQD device

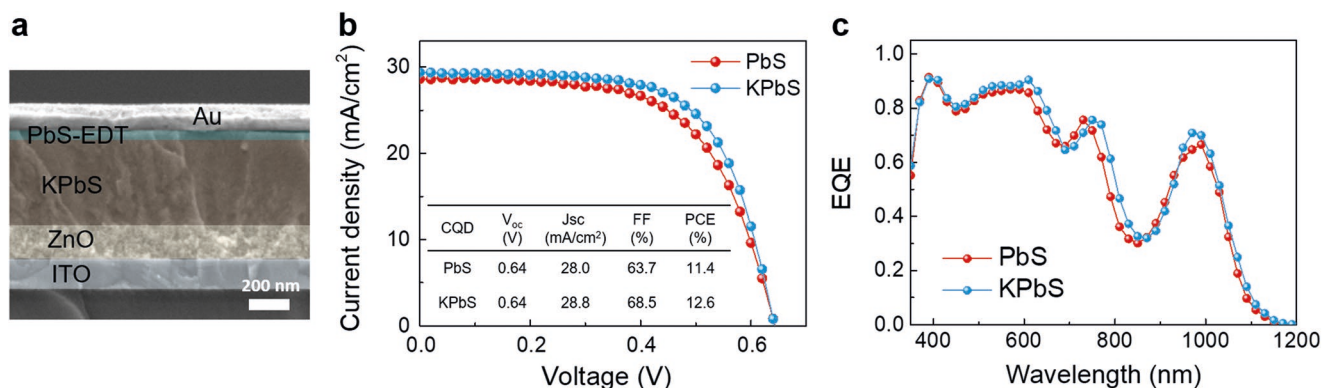


Figure 4. The effect of KPbS on CQD solar cell performance. a) Cross-sectional SEM image of a device consisting of ITO/ZnO/KPbS/PbS-EDT/Au. b) J - V characteristics and c) external quantum efficiency (EQE) of devices prepared using 1.32 eV bandgap PbS CQDs and KPbS CQDs.

during 50 h of MPP aging under air, whereas control PbS CQD devices retained 75% of their initial performance (Figure 5b,c). The KPbS devices retained $\approx 80\%$ of their initial efficiency following 300 h of MPP aging, the highest MPP stability reported among CQD PV devices (Figure 5c). The J - V characteristics of KPbS devices as a function of MPP aging time are detailed in Figure S5 (Supporting Information). XPS results reveal that the KPbS CQD films retain more iodide passivation and less oxides on their surfaces than do control PbS CQD films (Figure 5d and Figure S6, Supporting Information).

Here we demonstrate CQD PV devices that are stable under continuous operation in an air ambient. The improvements are traced to the use of KI shielding. This protects both the CQDs and the surface passivation from oxidation. Devices with KI shielding layer retain 80% of their initial performance following 300 h of device operation at MPP, while control devices retain the same relative performance for only 21 h at MPP. KI shielding maximizes the density of iodide on the surface and contributes to higher device performance (PCE, 12.6%) compared controls (PCE, 11.4%).

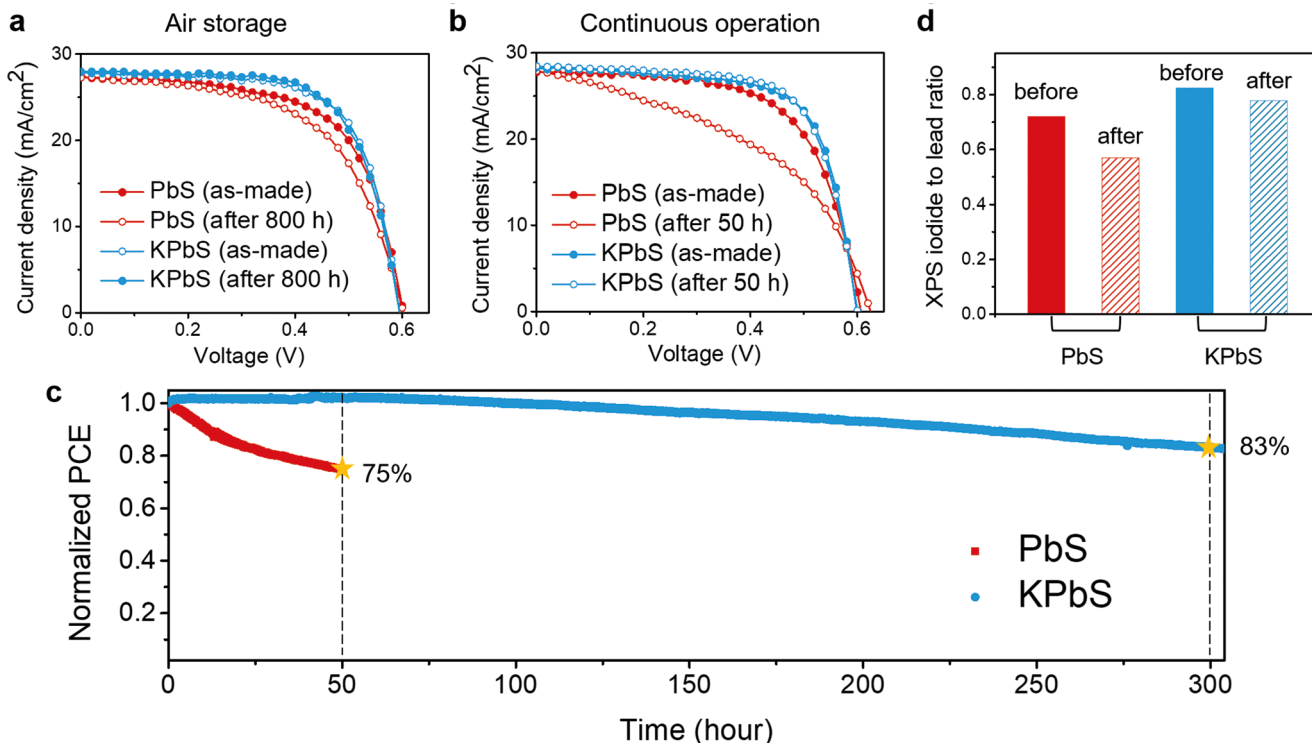


Figure 5. Stability test of CQD PV devices. a,b) J - V characteristics of CQD PV devices after being stored in air (a) and MPP tracking in air (b). c) Continuous device operation at MPP in air ambient. All devices are unencapsulated, and MPP tracking was performed under continuous 1 sun illumination, $50 \pm 10\%$ relative humidity, and at room temperature. d) Atomic iodide to lead ratio of PbS CQD films and KPbS CQD films before and after AM1.5 illumination for 10 h in air.

Experimental Section

Synthesis of PbS and KPbS CQDs: Lead iodide passivated PbS (control) CQDs were synthesized from oleic-acid-capped CQDs (OA-CQDs) via solution-phase ligand-exchange method under air by following reported methods.^[12] For the ligand exchange solution, lead iodide (0.1 M PbI₂), lead bromide (0.02 M PbBr₂), and NH₄Ac (0.04 M) were dissolved in dimethylformamide (DMF) solution. To produce KPbS, additional KI (0.01–0.05 M) was introduced into the ligand exchange solution. 5 mL of OA-CQDs dissolved in octane (10 mg mL⁻¹) were introduced into the as-prepared ligand exchange solution. Following 2 min vortexing of the solution, CQDs in octane had transferred into DMF. The CQD transferred (ligand-exchanged) solution was washed three times using octane to remove residues. The ligand-exchanged CQDs were collected by precipitating with the addition of toluene and drying under vacuum for 20 min. All the ligand exchange procedures were performed under ambient atmosphere.

Fabrication of CQD PV Devices: All device fabrication was performed under ambient atmosphere. ITO glass was cleaned using detergent, distilled water, isopropyl alcohol, and acetone. The ZnO nanoparticle and sol-gel ZnO films were synthesized using reported methods.^[12,17] ZnO solutions were spin-cast on rinsed ITO glass at 3000 rpm for 30 s. The PbS (or KPbS) CQDs dissolved in BTA were spin-coated onto ZnO substrates at 2500 rpm for 30 s. Two layers of EDT-PbS film were then spin-coated on top of PbS (or KPbS) CQD films by following reported protocols. For the top electrode, 120 nm Au was thermally evaporated on the PbS CQD film.

Characterizations of Photovoltaics: Current–voltage characteristics of CQD PV devices were measured using a Keithley 2400 source-meter under AM 1.5G illumination at intensity 100 mW cm⁻². The light intensity was calibrated with the aid of a reference Si solar cell (Newport). EQE spectra were taken using monochromated illumination from a 400 W Xe lamp passed through a monochromator and cutoff filters, corrected with the aid of Newport 818-UV and Newport 838-IR photodetectors. The photocurrent response was obtained using a Lakeshore preamplifier connected to a Stanford Research 830 lock-in amplifier. The stability test at continuous MPP operation under 1 sun, AM 1.5G illumination was studied in an air ambient (50 ± 10% relative humidity) at room temperature by fixing the voltage at V_{MPP} and then tracking the current output.

DFT Calculations: DFT calculations were performed using the Quickstep module^[30] in CP2K software. The calculations were performed using the Molopt DZP basis set^[31] along with Godecker–Teter–Hutter pseudopotentials,^[32] PBE exchange-correlation functional^[33] and a 300 Ry grid cutoff. PbS CQDs of ≈2.5 nm diameter (≈350 atoms) were calculated within a (5 nm)³ box. The structures were prepared in a rocksalt structure, where the surface was then passivated with either KI or I ligands, and then fully relaxed. The number of atoms of each type was adjusted to conform to the charge neutrality condition^[34] in order to avoid trap states in the bandgap.

Transient Photovoltage Measurements: The devices were biased with white light to reach near V_{oc} conditions and photoexcited with low power laser (500 nm) pulses to generate small photovoltage perturbations (ΔV kept to lower than 30 mV). Monoexponential fits to normalized traces were used to estimate the carrier lifetime at V_{oc} conditions.

FET Fabrication: Bottom-gate top-contact FET configuration was used as follows: 70 nm of titanium gate was thermally evaporated onto a glass substrate, followed by 15 nm of ZrO₂ as a dielectric layer using atomic layer deposition. After 300 °C baking for 1 h, the CQD solids were deposited onto the substrate. Then 70 nm of Au source/drain electrodes were thermally deposited using an Angstrom Engineering Amod deposition system. An Agilent 4155c semiconductor analyzer was used to characterize the FET devices.

Materials Characterization: XPS analysis was performed using a Thermo Scientific K-Alpha XPS system (300 μm spot size, 75 eV pass energy, and 0.05 eV energy steps). The XPS spectra were calibrated to the C 1s peak at a binding energy of 284.8 eV. A Lambda 950 500 UV–vis–IR spectrophotometer was used for optical absorption measurements. Field-emission scanning electron microscopy (SEM) (Hitachi SU8230) was employed to identify morphological characteristics of CQD PVs. PL

spectra were obtained using a Horiba Fluorolog time-correlated single-photon-counting system with photomultiplier tube detectors. The PL lifetime data was recorded on using a time-correlated single-photon counting system (Horiba).

Supporting Information

Supporting Information is available from the Wiley Online Library or from the author.

Acknowledgements

J.C., M.-J.C., and J.K. contributed equally to this work. The authors acknowledge the financial support from QD Solar. This work was supported by Ontario Research Fund-Research Excellence program (ORF7-Ministry of Research and Innovation, Ontario Research Fund-Research Excellence Round 7), and by the Natural Sciences and Engineering Research Council (NSERC) of Canada. J.C. received financial support by the DGIST Start-up Fund Program of the Ministry of Science, ICT and Future Planning (2019010116), and by the National Research Foundation of Korea (NRF) grant funded by the Korea government (MSIT) (NRF-2019R1G1A1099673). Computations were performed using the Niagara supercomputer at the SciNet HPC Consortium.^[35] SciNet is funded by the Canada Foundation for Innovation, the Government of Ontario, the Ontario Research Fund—Research Excellence, and the University of Toronto.

Conflict of Interest

The authors declare no conflict of interest.

Keywords

colloidal quantum dots, continuous operation, device stability, oxidation, solar cells

Received: October 3, 2019

Revised: November 22, 2019

Published online:

- [1] S. A. McDonald, G. Konstantatos, S. Zhang, P. W. Cyr, E. J. D. Klem, L. Levina, E. H. Sargent, *Nat. Mater.* **2005**, *4*, 138.
- [2] O. E. Semonin, J. M. Luther, S. Choi, H. Y. Chen, J. Gao, A. J. Nozik, M. C. Beard, *Science* **2011**, *334*, 1530.
- [3] W. K. Bae, J. Joo, L. A. Padilha, J. Won, D. C. Lee, Q. Lin, W.-K. Koh, H. Luo, V. I. Klimov, J. M. Pietryga, *J. Am. Chem. Soc.* **2012**, *134*, 20160.
- [4] V. M. Wood, J. Panzer, J. Chen, M. S. Bradley, J. E. Halpert, M. G. Bawendi, V. Bulović, *Adv. Mater.* **2009**, *21*, 2151.
- [5] K. Jeonghun, K. B. Wan, D. G. Lee, I. Park, J. Lim, M. Park, H. Cho, H. Woo, D. Y. Yoon, K. Char, S. Lee, C. Lee, *Nano Lett.* **2012**, *12*, 2362.
- [6] S. Y. Jeong, S. C. Lim, D. J. Bae, Y. H. Lee, H. J. Shin, S.-M. Yoon, J. Y. Choi, O. H. Cha, M. S. Jeong, D. Perello, M. Yun, *Appl. Phys. Lett.* **2008**, *92*, 243103.
- [7] S. Yang, N. Zhao, L. Zhang, H. Zhong, R. Liu, B. Zou, *Nanotechnology* **2012**, *23*, 255203.
- [8] G. Konstantatos, I. Howard, A. Fischer, S. Hoogland, J. Clifford, E. Klem, L. Levina, E. H. Sargent, *Nature* **2006**, *442*, 180.
- [9] J.-S. Lee, M. V. Kovalenko, J. Huang, D. S. Chung, D. V. Talapin, *Nat. Nanotechnol.* **2011**, *6*, 348.

- [10] A. H. Ip, S. M. Thon, S. Hoogland, O. Voznyy, D. Zhitomirsky, R. Debnath, L. Levina, L. R. Rollny, G. H. Carey, A. Fischer, K. W. Kemp, I. J. Kramer, Z. Ning, A. J. Labelle, K. W. Chou, A. Amassian, E. H. Sargent, *Nat. Nanotechnol.* **2012**, *7*, 577.
- [11] C.-H. M. Chuang, P. R. Brown, V. Bulović, M. G. Bawendi, *Nat. Mater.* **2014**, *13*, 796.
- [12] M. Liu, O. Voznyy, R. Sabatini, F. P. Garcia de Arquer, R. Munir, A. H. Balawi, X. Lan, F. Fan, G. Walters, A. R. Kirmani, S. Hoogland, F. Laquai, A. Amassian, E. H. Sargent, *Nat. Mater.* **2017**, *16*, 258.
- [13] J. Choi, Y. Kim, J. W. Jo, J. Kim, B. Sun, G. Walters, F. P. Garcia de Arquer, R. Quintero-Bermudez, Y. Li, C. S. Tan, L. N. Quan, A. P. T. Kam, S. Hoogland, Z. Lu, O. Voznyy, E. H. Sargent, *Adv. Mater.* **2017**, *29*, 1702350.
- [14] A. G. Pattantyus-Abraham, I. J. Kramer, A. R. Barkhouse, X. H. Wang, G. Konstantatos, R. Debnath, L. Levina, I. Raabe, M. K. Nazeeruddin, M. Gratzel, E. H. Sargent, *ACS Nano* **2010**, *4*, 3374.
- [15] G.-H. Kim, B. Walker, H.-B. Kim, J. Y. Kim, and E. H. Sargent, J. Park, *Adv. Mater.* **2014**, *26*, 3321.
- [16] M.-J. Choi, S. Kim, H. Lim, J. Choi, D. M. Sim, S. Yim, B. T. Ahn, J. Y. Kim, Y. S. Jung, *Adv. Mater.* **2016**, *28*, 1780.
- [17] J. Choi, J. W. Jo, F. P. G. Arquer, Y.-B. Zhao, B. Sun, J. Kim, M.-J. Choi, S.-W. Baek, A. H. Proppe, A. Seifitokaldani, D.-H. Nam, P. Li, O. Ouellette, Y. Kim, O. Voznyy, S. Hoogland, S. O. Kelley, Z.-H. Lu, E. H. Sargent, *Adv. Mater.* **2018**, *30*, 1801720.
- [18] J. Xu, O. Voznyy, M. Liu, A. R. Kirmani, G. Walters, R. Munir, M. Abdelsamie, A. H. Proppe, A. Sarkar, F. P. Garcia de Arquer, M. Wei, B. Sun, M. Liu, O. Ouellette, R. Quintero-Bermudez, J. Li, J. Fan, L. Quan, P. Todorovic, H. Tan, S. Hoogland, S. O. Kelley, M. Stefk, A. Amassian, E. H. Sargent, *Nat. Nanotechnol.* **2018**, *13*, 456.
- [19] Z. Ning, O. Voznyy, J. Pan, S. Hoogland, V. Adinolfi, J. Xu, M. Li, A. R. Kirmani, J.-P. Sun, J. Minor, K. W. Kemp, H. Dong, L. Rollny, A. Labelle, G. Carey, B. Sutherland, I. Hill, A. Amassian, H. Liu, J. Tang, O. M. Bakr, E. H. Sargent, *Nat. Mater.* **2014**, *13*, 822.
- [20] J. Y. Woo, J.-H. Ko, J. H. Song, K. Kim, H. Choi, Y.-H. Kim, D. C. Lee, S. Jeong, *J. Am. Chem. Soc.* **2014**, *136*, 8883.
- [21] J. Zhang, J. Gao, E. M. Miller, J. M. Luther, M. C. Beard, *ACS Nano* **2014**, *8*, 614.
- [22] S.-W. Baek, S. H. Lee, J. H. Song, C. Kim, Y. S. Ha, H. Shin, H. Kim, S. Jeong, J. Y. Lee, *Energy Environ. Sci.* **2018**, *11*, 2078.
- [23] Y. Cao, A. Stavrinadis, T. Lasanta, D. So, G. Konstantatos, *Nat. Energy* **2016**, *1*, 16035.
- [24] X. Zhang, J. Zhang, D. Phuyal, J. Du, L. Tian, V. A. Öberg, M. B. Johansson, U. B. Cappel, O. Karis, J. Liu, H. Rensmo, G. Boschloo, E. M. J. Johansson, *Adv. Energy Mater.* **2018**, *8*, 1702049.
- [25] J. Tang, L. Brzozowski, D. A. R. Barkhouse, X. Wang, R. Debnath, R. Wolowicz, E. Palmiano, L. Levina, A. G. Pattantyus-Abraham, D. Jamakosmanovic, E. H. Sargent, *ACS Nano* **2010**, *4*, 869.
- [26] A. Stavrinadis, G. Konstantatos, *ChemPhysChem* **2016**, *17*, 632.
- [27] M.-J. Choi, J. Oh, J.-K. Yoo, J. Choi, D. M. Sim, Y. S. Jung, *Energy Environ. Sci.* **2014**, *7*, 3052.
- [28] N. Zhao, T. P. Osedach, L.-Y. Chang, S. M. Geyer, D. Wanger, M. T. Binda, A. C. Arango, M. G. Bawendi, V. Bulovic, *ACS Nano* **2010**, *4*, 3743.
- [29] D. Zhitomirsky, O. Voznyy, S. Hoogland, E. H. Sargent, *ACS Nano* **2013**, *7*, 5282.
- [30] J. VandeVondele, M. Krack, F. Mohamed, M. Parrinello, T. Chassaing, J. Hutter, *Comput. Phys. Commun.* **2005**, *167*, 103.
- [31] J. VandeVondele, J. Hutter, *J. Chem. Phys.* **2007**, *127*, 114105.
- [32] C. Hartwigsen, S. Goedecker, J. Hutter, *Phys. Rev. B* **1998**, *58*, 3641.
- [33] J. P. Perdew, K. Burke, M. Ernzerhof, *Phys. Rev. Lett.* **1996**, *77*, 3865.
- [34] O. Voznyy, D. Zhitomirsky, P. Stadler, Z. Ning, S. Hoogland, E. H. Sargent, *ACS Nano* **2012**, *6*, 8448.
- [35] C. Loken, D. Gruner, L. Groer, R. Peltier, N. Bunn, M. Craig, T. Henriques, J. Dempsey, C.-H. Yu, J. Chen, L. J. Dursi, J. Chong, S. Northrup, J. Pinto, N. Knecht, R. V. Zon, *J. Phys.: Conf. Ser.* **2010**, *256*, 012026.